Multifractality and randomness in the unstable plastic flow near the lower strain-rate boundary of instability

M. A. Lebyodkin[1,*] and T. A. Lebedkina[2,3,†]

[1]*Laboratoire de Physique et Mécanique des Matériaux, UMR CNRS No 7554, Université Paul Verlaine - Metz, Ile du Saulcy, 57045 Metz Cedex, France*

[2]*Institute of Solid State Physics, Russian Academy of Sciences, 142432 Chernogolovka, Russia*

[3]*Laboratoire de Physique des Matériaux, UMR CNRS-UHP-INPL No 7556, Ecole des Mines de Nancy, Parc de Saurupt, 54042 Nancy cedex, France*

(Received 20 August 2007; published 15 February 2008)

The unstable plastic flow of an AlMg alloy, associated with the Portevin-Le Chatelier effect, was studied near the lower strain-rate boundary of instability using multifractal analysis. Self-similarity of deformation curves, indicating long-range time correlations of stress serrations, was detected within the strain-rate range where serrations are commonly ascribed to the occurrence of uncorrelated deformation bands. The deformation curves display a wide range of shapes that are characterized by different groupings of serrations. Multifractal analysis provides a method to quantify the observed complexity and compare it to known Portevin–Le Chatelier effect regimes. The measurement noise effect on the multifractal spectra determined from experimental data was mimicked by superposing multifractal Cantor sets with random noise. Such tests using standard multifractal data sets justify the separation of self-similar and random components of the serrated deformation curves. Furthermore, these results shed light on the general problem of the effect of experimental noise on the apparent multifractal properties of physical fractals.

DOI: 10.1103/PhysRevE.77.026111 PACS number(s): 62.20.F−, 05.45.Tp, 05.45.Df, 83.60.Wc

I. INTRODUCTION

The discontinuous plastic flow of alloys associated with the Portevin–Le Chatelier (PLC) effect [1] is an example of a collective phenomenon akin to relaxation oscillations [2] in other complex nonlinear systems. Indeed, the dynamical nature of this effect can be illustrated by the following qualitative consideration. The microscopic mechanism of plastic deformation during the PLC effect is dislocation glide, which is governed by thermally activated motion of dislocations past obstacles. Increasing the plastic strain rate requires a decrease in the waiting time associated with the thermal activation of dislocations. In the case of a pure metal deformed at a constant temperature, this is equivalent to a requirement of increasing the applied stress. The mechanical behavior for pure materials is often described by positive stress-rate relationships, which result in stable plastic deformation and macroscopically smooth deformation curves. In solution-strengthened alloys, the resistance to further motion of dislocations temporarily arrested at obstacles increases by solute atoms diffusing to them during the waiting time. For these materials, the reduction of waiting time may lead to a depletion of the solute concentration on the arrested dislocations and consequently decreases the required stress for further slip. As a result, the dependence of the flow stress on the strain rate is *N* shaped for many alloys, with a typical range of negative strain-rate sensitivity from 10^{-6} to 10^{-2} s^{-1}. Deformation of such alloys is essentially a process of relaxation oscillations, providing that the applied strain rate is chosen within the aforementioned range. The plastic flow experiences recurrent accelerations via activation of deformation bands [3,4]. In particular, this leads to the observation of repetitive unloading or serration in experiments conducted at a constant strain rate.

The strain heterogeneity in real materials is more complex than an idealized picture based on the suggestion that all dislocations behave equally. Specifically, the serrations are not periodic and the deformation curves display a variety of shapes depending on the material and testing conditions. However, several common types of stress serrations and deformation band patterns have been observed for various materials and related to certain experimental conditions [5]. This suggests that the plastic flow has a nonrandom character, which may reflect the collective dislocation dynamics [3]. In particular, the correlation of the deformation bands becomes weaker when the applied strain rate is decreased, as expected from the phenomenological classification of the PLC effect. Characterizations of the instability observed at different applied strain rates often fall into the following categories. A quasicontinuous propagation of deformation bands is observed near the upper strain-rate boundary of plastic instability (the so-called type *A* behavior). It changes to "relay-race" propagation; successive formation of distinct bands in the vicinity of each other at intermediate strain rates (type *B* behavior). Finally, the bands are commonly believed to nucleate at random near the lower instability boundary (type *C* behavior).

Earlier studies have shown that types *A* and *B* of the PLC effect are related to distinct dynamical regimes. Specifically, power-law statistics were found for the amplitudes and intervals between type *A* stress jumps [6,7]. The scale invariance of the distributions, expressed by the power law, was as-

*On leave from: Institute of Solid State Physics, Russian Academy of Sciences, 142432 Chernogolovka, Russia. lebedkin@univ-metz.fr

†tlebyod@issp.ac.ru

cribed to avalanchelike motion of dislocations, akin to self-organized criticality in extended nonlinear systems [8]. In contrast, low-dimensional chaotic behavior was detected by reconstructing phase-space trajectories for type *B* deformation curves [7,9]. The reconstructed strange attractors—a signature of chaos—are also characterized by scale invariance associated with their geometry [10]. Moreover, since the transition between two kinds of dynamics can be controlled by a single parameter, e.g., the applied strain rate, the plastic instability presents a particularly interesting example of nonlinear dynamics.

Neither the statistical analysis nor the phase space reconstruction revealed a particular dynamical character for type *C* effect. Several other approaches, also based on searching for scaling laws characterizing the intermittent plastic flow, have been proposed recently (e.g., [11–14]). However, these works concentrated on higher strain rates. Furthermore, the quantitative analysis of type *C* behavior is complicated by a diversity of shapes associated with type *C* deformation curves. This observation supports the notion that type *C* serrations exhibit a stochastic nature, which slowed down the progress toward understanding the low strain-rate domain of instability. Nevertheless, a recent investigation utilizing the multifractal analysis of deformation curves indicates that the PLC effect may manifest scale-invariant behaviors throughout the entire range of strain rates, including the type *C* domain [15]. This conclusion contradicts the previous hypothesis and warrants a more detailed investigation.

This paper reports the results of a multifractal analysis of type *C* instability in an AlMg alloy and is organized as follows. Section II describes experimental details and outlines the multifractal approach to analyze the serrated deformation curves. The application of this analysis to the experimental data is presented in Sec. III. It is shown that the serration sequences contain both random serrations and a correlated component that results in scaling laws. To verify this conclusion, the same analysis is applied in Sec. IV to hypothetical signals obtained by superposing white noise on multifractal Cantor sets. The proposed multifractal analysis is found to be capable of revealing the correlated behavior even with the presence of a high noise level component.

II. EXPERIMENTAL TECHNIQUE AND DATA ANALYSIS

Flat polycrystalline specimens of an AlMg (3 at. % Mg) alloy with the gauge dimensions of $20\times5.5\times1.5$ mm^3 were pulled in tension at room temperature at a constant strain rate. All specimens were annealed at 400 °C for 2 h and quenched in water to provide a uniform solute concentration, which avoids an extrinsic source of material heterogeneity. Most experiments were carried out at a low strain rate, $\dot{\varepsilon}_a=4\times10^{-6}$ s^{-1}, assuring type *C* behavior. It was checked that the transition to type *B* instabilities occurred above $\dot{\varepsilon}_a=2\times10^{-5}$ s^{-1}. Additional tests were conducted at strain rates of 2×10^{-6} s^{-1} and 6×10^{-4} s^{-1}. The data acquisition rate was chosen between 0.5–250 Hz, depending on $\dot{\varepsilon}_a$, such that the files for the multifractal analysis contained between 10 000 to 40 000 data points. A procedure, similar to that used in [16], was employed to verify that reducing the size of the original data files by factors of two or four did not significantly modify the multifractal characteristics.

The application of the multifractal analysis [17,18] to jumplike deformation curves has been described in several papers [7,15,16] and will be subsequently outlined. First, a stress-time curve $\sigma(t)$ is normalized to allow for slow trends (corresponding to the test duration) due to strain hardening [16]. The relevant time series, reflecting the plastic instability events, is obtained by finding the absolute value of the finite difference approximation $\psi_j(t_j)$ for the derivative $d\sigma(t)/dt$ of the normalized curve. The data set $\psi_j(t_j)$ is covered with grids with the division δt that varies as powers of 2. For a given δt, a probability measure $\mu_i(\delta t)$ is calculated as the normalized sum of ψ magnitudes in the ith interval δt:

$$\mu_i(\delta t)=\sum_{k=1}^{n}\psi_k\Big/\sum_{j=1}^{N}\psi_j, \tag{1}$$

where N is the total number of the data points and n the number of points in the ith interval. With this definition, the measure μ_i characterizes the intensity of plastic instabilities within a given time range.

The qth moment of the measure, defined as $Z_q(\delta t)=\Sigma_i\mu_i^q$, is calculated for various q values (q is a real number; see Ref. [19] for the particular case $q=1$). To demonstrate how the family of $Z_q(\delta t)$ dependences describes the scaling properties of a time series, it is convenient to consider a trivial example of scale invariance, a constant signal. In this case, the corresponding uniform measure μ_i is simply proportional to δt. The number of terms in the summation in Eq. (1) is given by the number of δt intervals, which scales as δt^{-1} in the limit $\delta t\to0$. Thus the scaling dependences follow power-law behavior, $Z_q(\delta t)\sim\delta t^{q-1}$, when δt is small enough compared to the signal duration. This example is interesting because similar attributes also result from the analysis of random or periodic stress drops. Indeed, these events are uniformly distributed in time above some characteristic period. If the time series is long enough, the trivial scaling law will be followed over certain δt intervals, which are restricted by the characteristic period at small scales and the total time at large scales.

For a multifractal structure, the $Z_q(\delta t)$ dependences can be described by a similar relationship,

$$Z_q(\delta t)\sim\delta t^{(q-1)D_q}, \tag{2}$$

where the values of D_q generally depend on q and differ from unity (cf. [19] for $q=1$). In particular, a uniform fractal structure corresponds to a unique but a nontrivial scaling law. This behavior unambiguously proves the presence of long-range correlations in the corresponding data set. As was previously shown [7,15], the spectrum of generalized fractal dimensions D_q of PLC deformation curves change for various PLC types. Thus, the fractal dimensions can characterize the respective changes governing the dislocation dynamics.

A few D_q values have a direct interpretation [18]. Particularly, $Z_0(\delta t)$ is the number of cells with a nonzero measure, consequently, D_0 is the box-counting estimate of the fractal dimension (or capacity), which characterizes the geometrical support of the stress serrations. However, there is no general

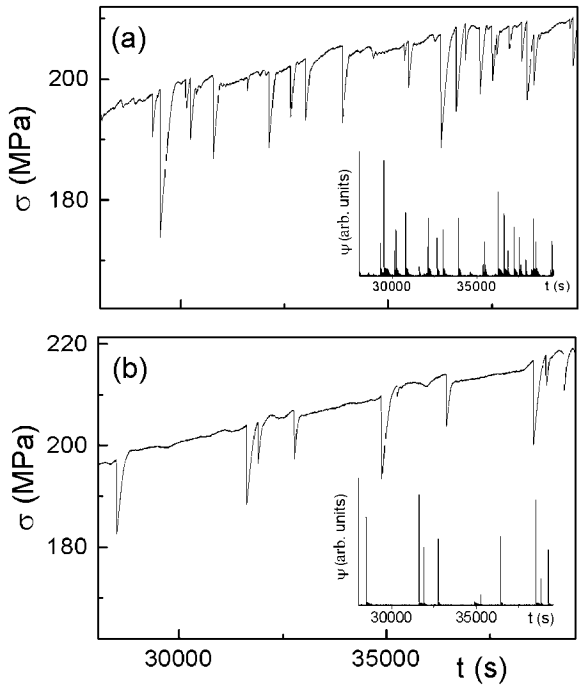

FIG. 1. Examples of portions of stress-time curves $\sigma(t)$ of AlMg polycrystalline samples deformed at a strain rate of 4×10^{-6} s^{-1}. Insets: Corresponding plots of $\psi=|d\sigma(t)/dt|$.

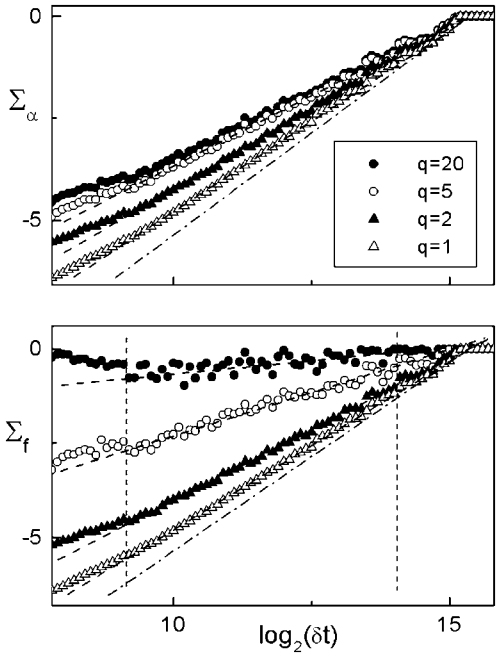

FIG. 2. Examples of scaling dependences (3) for the time series shown in Fig. 1(a). Vertical dashed lines bound the intervals used to calculate the multifractal spectra; dashed lines trace the corresponding average slopes; dashed and dotted lines trace the unit slope that would be found at all q values in the uniform case, e.g., for a stochastic series.

interpretation of various D_q magnitudes. This difficulty is caused by the global character of Z_q sums, which mix powers of μ_i's throughout the data set. It is useful to consider an equivalent representation for characterization that partitions local scaling indices. As a result, the scaling law (2) is related to the scaling of the local measure itself: $\mu_i(\delta t)\sim\delta t^{\alpha}$, where α is a local characteristic that can have a continuous range of values in the limit as $\delta t\to0$, with $\alpha<1$ reflecting singular behavior [17]. Further, the data subsets corresponding to neighboring values of α are fractal and can be quantified by their capacities f. The singularity spectrum so obtained, $f(\alpha)$, is unambiguously related to the D_q dependence by the Legendre transformation [17]. In this investigation, $f(\alpha)$ was determined using scaling relationships suggested in [20],

$$\Sigma_\alpha(\delta t,q)=\sum_i \tilde{\mu}_i(\delta t,q)\ln\,\mu_i(\delta t)\sim\alpha(q)\ln\,\delta t,$$

$$\Sigma_f(\delta t,q)=\sum_i \tilde{\mu}_i(\delta t,q)\ln\,\tilde{\mu}_i(\delta t,q)\sim f(q)\ln\,\delta t, \qquad (3)$$

where $\tilde{\mu}_i(\delta t,q)=\mu_i^q/\Sigma_j\mu_j^q$, which avoids numerical derivation difficulties encountered when using the Legendre transformation. Both spectra, D_q and $f(\alpha)$, were traced by varying q from −20 to 40. The slopes of the scaling dependences for each q were estimated by averaging over ten trials with randomly chosen starting points utilized to generate the δt grid.

III. EXPERIMENTAL RESULTS AND DISCUSSION

The deformation curves recorded at the strain rate of 4×10^{-6} s^{-1} possessed cognate type C features, namely deep stress drops (from a few MPa to about 30 MPa) followed by a much smoother reloading portion, as illustrated in Fig. 1. The experimental measurement noise, which has an amplitude of approximately 0.1 MPa, is also discernible on the smoother portions of the curves. In spite of the qualitative similarity, the examples in Fig. 1 illustrate that the stress evolution can vary strongly between samples. The deformation curves are characterized by different dispersions of stress jump amplitudes and the variable clustering of these events. Indeed, the stress jumps in Fig. 1(a) occur throughout the range of deformation and display a variety of amplitudes above the measurement noise level. In contrast, Fig. 1(b) shows distinct events that clearly form clusters, which suggests correlation of the deformation processes.

Such a clear visual distinction is not obvious for all specimens. Thus a quantitative approach that provides a characterization of the temporal structure for various deformation curves is needed. Multifractal analysis proves to be a suitable technique, since the scaling dependences described by Eqs. (2) and (3) are found for most deformation curves. The analysis demarked two typical experimental situations corresponding to the examples presented in Fig. 1. These cases will be discussed in detail below.

Figure 2 presents examples of scaling dependences [Eq. (3)] for the curve displayed in Fig. 1(a). A linear region is apparent over an interval ranging from approximately 500 s to at least 20 000 s (it almost persists to the entire duration, 37 000 s, of the deformation curve) and allows a reliable determination of the respective slopes. The scaling ranges for similar deformation curves included intervals starting be-

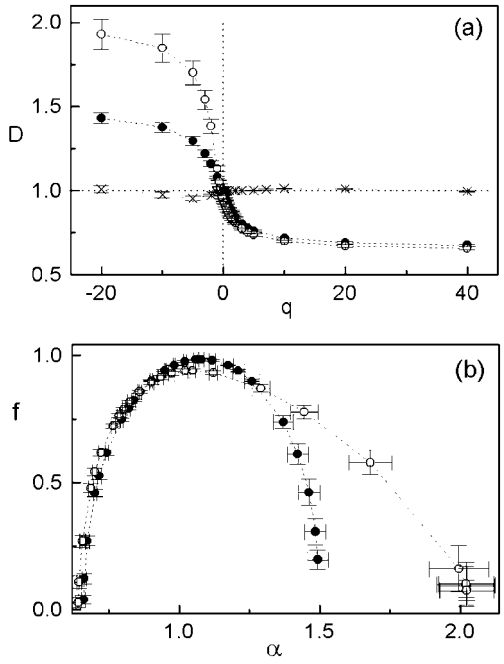

FIG. 3. (a) Generalized dimension and (b) singularity spectra for the time series shown in Fig. 1(a). Solid circles—the entire data set; open circles—after cutting off the bursts below $\psi_{thr}=0.03\psi_{max}$. The horizontal dotted line in the above figure represents the spectrum in the ideal uniform case [it would correspond to a single point (1;1) in the bottom figure]. For comparison, the generalized dimension spectrum for a random set is shown (crosses).

tween 200 and 500 s and ending between 20 000 and 30 000 s. It can be seen in Fig. 2 that the slopes gradually change with varying q, revealing a multifractal character of the time series. The resulting spectra D_q and $f(\alpha)$ are presented in Fig. 3. The error bars shown in the figure were determined from least-square estimates of the slope's standard deviation. In the general case, all kinds of uncertainty contribute to the data scatter on scaling dependences: The finite number of events in the experimental dataset, the inevitable noise and measurement errors, and possible nonfractal components. Therefore, the applied procedure naturally incorporates the stress measurement error (see also [18,21] for evaluation of the error of determination of fractal dimensions from experimental data). The spectra in Fig. 3 are characteristic of multifractal structures [17]. For comparison, Fig. 3(a) also presents a dependence D_q calculated for a numerically generated random time series containing 2^{14} data points. As shown, the random case is close to the ideal case of a perfectly uniform measure (horizontal line $D_q=1$).

Since the upper scaling bound is near the total test duration, long-range time correlations between stress jumps were identified. On the other hand, the lower scaling bound shows that the multifractal behavior may not extend to small time scales, which reflect the characteristic range of interevent times between small stress irregularities with amplitudes below ~1 MPa. It can be suggested that the observation of the scale-invariant behavior is strongly affected by the correlation between large plastic flow events. This suggestion is supported by the evaluation of truncated data sets, which remove the low-amplitude part of the time series using a threshold with an increasing magnitude ψ_{thr}. Changes in the spectra were found to be insignificant while ψ_{thr} is less than $\sim 0.03\psi_{max}$, which corresponds to a stress drop amplitude of ~1 MPa (the maximum value ψ_{max} considers the entire time series). The results of the truncation test for $\psi_{thr}=0.03\psi_{max}$ are also illustrated in Fig. 3. It is apparent that only the data for negative q values are considerably influenced by the signal truncation. As follows from Eqs. (2) and (3), the lesser values of the measure μ dominate Z_q sums when $q<0$ [17]. Therefore, it is not surprising that the respective spectra branches are perturbed by the removal of small events. In contrast, the spectra parts corresponding to non-negative q's, which are dominated by the largest local measure values, prove to be very robust. The values of α and D are slightly diminished by the truncation, which is expected due to the amplification of the local singularity when retaining only the largest local bursts. The dimension of the signal support, $D_0=f_{max}$ [18], is also weakly affected by truncation. The proximity of this value to unity ($D_0\approx 0.95$) indicates that the events responsible for the observation of multifractality are approximately uniformly distributed in time. This observation is also consistent with the effect of further increasing of ψ_{thr}: It does not lead to abrupt changes, but to a progressive deterioration of the scaling interval and dilatation of the spectra because of the depletion of event statistics in the data set.

These results show that the deformation curve is composed of both a self-similar structure and a nonfractal component. The latter includes stress jumps with amplitudes up to ~1 MPa, or an order of magnitude higher than the measurement noise, which is conform to the common conjecture of a stochastic nature of type C PLC effect. On the contrary, the intensive deformation bands affect subsequent events, leading to the long-range time correlations detected by the multifractal analysis. It should be also noted that the deviation from the scaling law at small scales may not mean that all the low-amplitude jumps are independent of the multifractal sequence. However, the analysis cannot distinguish the possible low-amplitude multifractal jumps from the random sequence.

The scaling dependences found for deformation curves with strong jump clustering [Fig. 1(b)] also showed linear regions with gradually changing slopes, which again suggest multifractality. However, the quantitative results are different from those discussed previously. The linear scaling was found over time intervals starting between 50 and 200 s and ending between 1500 and 3000 s, where the upper scaling bound matches the maximum length of the stress jump clusters. As shown in Fig. 4, the spectra obtained for the entire deformation curve presented in Fig. 1(b) pass through the points corresponding to $D_0\approx 1$. Although this result is similar to the corresponding data in Fig. 3, the dependences are nonmonotonic when $q<0$, which infers that one cannot unambiguously prove the multifractal character of the deformation curves. Such peculiarities will be further evaluated in Sec. IV using multifractal Cantor sets. Nevertheless, it turns out that the multifractal structure of the experimental data can be unmasked by truncation tests without recourse to hypothetical data sets. Similar to the above case, the multifrac-

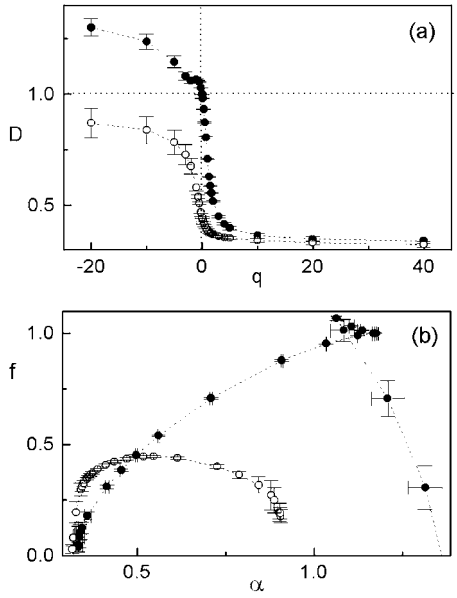

FIG. 4. Same as in Fig. 3 for the time series shown in Fig. 1(b). Solid circles—the entire data set; open circles—after cutting off the bursts below $\psi_{thr}=0.03\psi_{max}$.

tal spectra of highly clustered time series are not noticeably influenced by a truncation with $\psi_{thr}<0.03\psi_{max}$. However, they acquire smooth shapes (cf. Fig. 4) around $\psi_{thr}=0.03\psi_{max}$. The modified spectra are characteristic of singular and clustered behavior: $D_0\approx 0.45$ and $\alpha(q)<1$ for all q's in Fig. 4. It can be concluded that the large events form a self-similar structure that is more highly clustered that in the previous case. The effect of truncation can be easily understood. First, the initial signal is nonzero almost everywhere due to experimental noise, indicated by D_0's proximity to unity. Next, the nonmonotonic behavior at $q<0$ is the result of a mixture of the nonfractal and the multifractal components, where the smaller nonfractal component becomes significant in Z_q sums with decreasing q. Last the positive q branches, where the contribution associated with large stress bursts is dominant, are not significantly influenced by filtering small events and converge with the unmodified spectra at large q. The deterioration of the smooth spectra upon excessive truncation was similar to the prior observation for dense series and was primarily dominated by the depletion of the data set.

The data evaluation using multifractal analysis shows that the two visually different experimental situations are qualitatively similar and that some conclusions made for the nonclustered serration sequences are also valid for the clustered sequences. The agreement of the critical threshold and the correlation between the upper scaling bound and the maximum length of stress jump clusters (the test duration in the nonclustered case) testify that the self-invariant behavior can be primarily attributed to the larger stress jumps.

The variability of the multifractal characteristics between samples and the large width of the spectra suggest that the type C instabilities are highly heterogeneous. In the previous investigation (e.g., [7,15]), bursts of heterogeneity were observed over a strain-rate interval between type B to type A

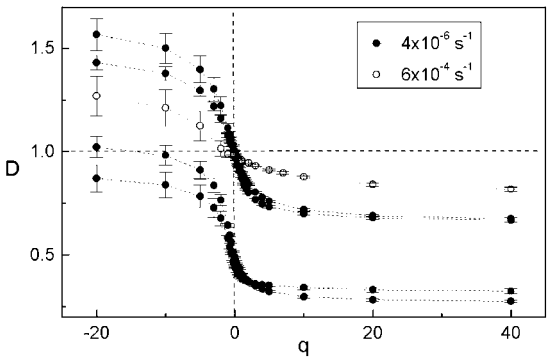

FIG. 5. Examples of generalized dimension spectra for four specimens deformed at the reference strain rate $\dot{\varepsilon}_a=4\times10^{-6}$ s^{-1} and a specimen deformed under type B conditions ($\dot{\varepsilon}_a=6\times10^{-4}$ s^{-1}).

behavior. Persistent narrow spectra, indicating a high degree uniformity, were found over a wide strain-rate range corresponding to the type B serration domain. In view of these observations, additional tests were conducted at strain rates below and above the reference strain rate of 4×10^{-6} s^{-1}. The spectra found at 6×10^{-4} s^{-1} (type B effect) were close to those reported in [16] for the same alloy composition and displayed narrower dependences than those in Figs. 3 and 4 (see Fig. 5). On the other hand, no multifractal characteristics were found for tests conducted at 2×10^{-6} s^{-1}. This strain rate resulted in regular type C deformation curves with roughly equally spaced deep stress jumps or, at most, pairs of jumps. The corresponding scaling dependences for various q's converged to the unique slope, $D_q=1$ (cf. Sec. II), for δt exceeding the interjump spacing. Therefore, it is natural to suggest that the heterogeneity observed at the reference strain rate is caused by a transitory behavior between type B serrations and periodic relaxation oscillations.

The microscopic mechanism of heterogeneity can be understood within the unique framework proposed in [6,7]. It considers a competition between triggering local strain jumps and the relaxation of prior heterogeneity via plastic flow during the subsequent reloading. Elastic mismatch, generated by local strain incompatibilities in polycrystalline materials, is usually considered as a driving force for plastic relaxation. At the limit of a very slow reloading, which tends to favor effective strain uniformity, this mechanism results in periodic relaxation oscillations associated with deformation bands occurring at random sites (cf. Sec. I). This assertion was confirmed by the tests at the slowest strain rate, $\dot{\varepsilon}_a=2\times10^{-6}$ s^{-1}. As strain rate increases, the reloading time becomes insufficient to completely relax the local strain differences, so periodicity is broken. It should be stressed that such a qualitative consideration cannot forecast whether the resulting irregularity consists of random fluctuations superposed on periodic oscillations or a deterministic structure that reflects the correlated dislocation motion. On the contrary, the multifractal analysis presented in this investigation confirms the suggestion made in [15], which postulated that long-range time correlations in a dynamic dislocation system operate over a broad range of strain rates, including both type B and type A PLC effects, as well as type C serrations.

Moreover, the proposed fractal analysis provides evidence that a unique dynamical mechanism is useful to examine the experimental variability of type *C* deformation curves. The key point is likely the variation of the internal stresses, which is controlled by the material microstructure. The deformation bands and the associated stress serrations would tend to cluster in a material with a homogeneous microstructure. Indeed, when the stress level is nearly uniform throughout the specimen, the internal stress increment due to a deformation band would trigger the next band in its neighborhood. In contrast, the band correlation weakens in heterogeneous materials, because a new band may develop in either a neighboring site due to the generated internal stresses, or elsewhere in the material due to independently achieving the instability condition. If the strain rate is high enough, the plastic relaxation of strain incompatibilities can become inefficient, and the bands will show high correlation in any material. Such behavior can be associated with type *B* serrations characterized by "relay-race" propagation of deformation bands throughout the specimen. Indeed, the multifractal characteristics of type *B* PLC effect were found to be weakly sensitive both to the strain rate and the material microstructure [7,15].

IV. INFLUENCE OF NOISE ON MULTIFRACTAL SETS

To verify the procedure used to unmask the multifractal structure and stochastic background associated with the experimentally observed behavior, multifractal Cantor sets, with deliberate noise contamination, were analyzed. The Cantor sets with variable clustering degrees were constructed by an iterative segment division procedure. At the first iteration, the segment is divided into i pieces storing the relative segment size l_i and the relative measure p_i [18]. At the proceeding steps, the fragmentation is repeated for all segments of the current construction such that their lengths are multiplicative combinations of l_i and their measures are multiples of p_i. The multifractal spectra are calculated according to the procedure described in Sec. II, using grids with the box length δl varied as powers of 2.

It was found that noise, which has a continuous support, only weakly affects the multifractal spectra of the Cantor set, providing that it is also distributed on the continuous support. A continuously distributed Cantor set was constructed using rescaling factors $l_i=\frac{1}{4}(i=1$ to $4)$, $p_1=\frac{1}{6}$, $p_2=p_3=\frac{1}{4}$, and $p_4=\frac{1}{3}$ (cf. [16]). Figure 6(a) presents the scaling dependences (2) for a set containing 2^{14} segments (thirteen iterations). The linear behavior is seen over approximately three orders of magnitude of δl, which allows a reliable determination of the multifractal spectra as demonstrated in Fig. 7. The calculated spectra and the analytical dependences coincide when $q>0$. Moreover, they show fair agreement in the range $q<0$, which corresponds to the regions with rarified measure and is poorly handled by the utilized numerical procedure [21]. The figure also illustrates that $D_0=1$, as expected for a data set with continuous support. Such a dense Cantor set turns out to be extremely robust with regard to noise. Although the addition of noise leads to a smaller interval of power-law scaling, depending on the noise amplitude, the data in Fig. 7 testify that the spectra can be reliably determined up to a noise level

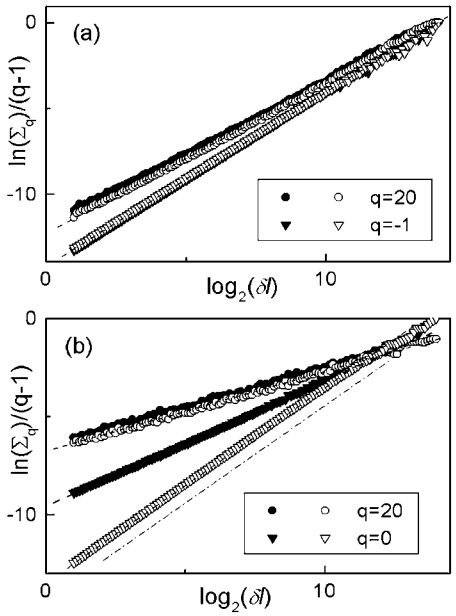

FIG. 6. Examples of scaling dependences [see relationship (2)] for multifractal Cantor sets distributed on a (a) continuous and (b) fractal geometrical support. Solid symbols—initial sets; open symbols—the same sets superimposed with random noise. The dashed and dotted line traces the unit slope. δl denotes the grid size.

of $(0.2-0.3)\psi_{\max}$. Moreover, the spectra also persist upon truncation, despite removing not only added noise but also portions of the initial Cantor set. Such robustness justifies the approach used to analyze the experimental data.

More complex behavior was found for a highly clustered Cantor set generated with the rescaling factors $l_1=0.25$, l_2

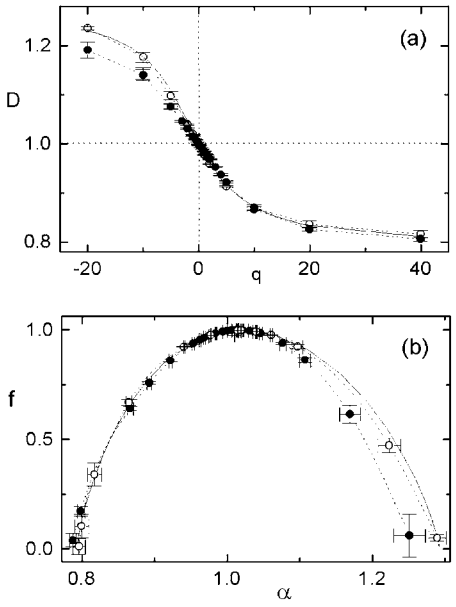

FIG. 7. (a) Generalized dimension and (b) singularity spectra of the multifractal Cantor set distributed on a continuous support (open circles) and the same set superposed with a 20% noise (solid circles). The solid line presents the analytical dependence for the initial set.

=0.35, l_3=0.4, p_1=0.6, p_2=0, and p_3=0.4 [17]. In this case, the clustering is provided by enforcing a zero measure to the middle segments, i.e., removing the midsections. The scaling dependences (2) for the set containing 2^{14} nonempty segments (fourteen iterations) are presented in Fig. 6(b). The respective multifractal spectra are shown in Fig. 8. The comparison with the analytical dependences shows that the calculation procedure is not independent of the previously mentioned imprecision for the subsets corresponding to small measure values (large systematic errors appear in the negative q range). However, the spectra are well determined for positive q's, which allows a study of the noise effect.

The fractal dimension D_0 of the highly clustered Cantor set is approximately equal to 0.62. It is obvious that the addition of any noise, even of very small amplitude, will strongly affect the multifractal spectra by changing from the fractal nature to a continuous support, where D_0 is exactly 1. This crossover is illustrated in Fig. 6(b) using the example of scaling dependences for noise at the level of $0.05\psi_{\max}$. For large positive q values, where the Cantor set elements dominate, the curves coincide with the dependences found in the absence of noise. However, the slope approaches 1 for q=0. Some bending of scaling dependences is observed at small q's because of significant contributions from the Cantor set and the noise. Nevertheless, for the selected array of q values, nonlinear behavior did not exceed data scatter. Thus, linearity was not completely deteriorated and the respective slopes could be determined. For q values slightly below zero, the increasing significance of the noise contribution leads to a nonmonotonic slope variation and other peculiarities of the spectra similar to those observed in experiments. The overall effect of noise is clear from the comparison of the spectra of the initial Cantor set and the perturbed set (Fig. 8). The differences between these spectra are remarkably similar to those observed in experiments after removing the low-amplitude component of the time series (cf. Figs. 4 and 8). It was verified that filtering the low-amplitude part of the noise-perturbed Cantor set effectively restored the initial spectra. These tests justify the hypothesis on the superposition of stochastic and multifractal components in the experimental data.

V. CONCLUSIONS

The PLC effect is an example of nonlinear dynamics, with a rare property that two distinct dynamical regimes—self-organized criticality and deterministic chaos—were observed in different strain-rate ranges [6,7,9]. Both regimes correspond to visible changes in the temporal structure of deformation curves. The transition between the high-dimension critical regime and the low-dimension chaotic regime takes place when the imposed strain rate is decreased. One more change, documented in the phenomenological classification of the PLC effect (type C serrations), occurs upon its further decrease. It is thus topical making a map of dynamical behaviors in the whole domain of plastic instability.

The multifractal analysis discloses self-similarity associated with type C deformation curves, which unambiguously proves the existence of long-term correlations of deformation

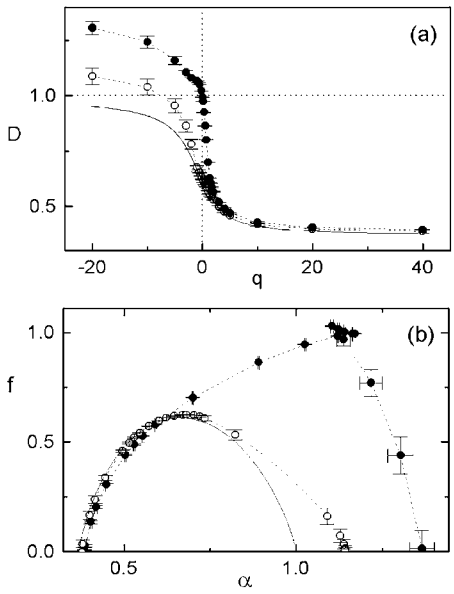

FIG. 8. (a) Generalized dimension and (b) singularity spectra of the clustered Cantor set (open circles) and the same set superposed with a 5% noise (solid circles). The solid line presents the analytical dependence for the initial set.

bands characteristic of the low strain-rate regime. Such correlations can be attributed to successive band initiation and the occurrence of long-range internal stresses. The exact shapes of the serration sequences and their corresponding multifractal spectra are quite diverse. This variation is likely to be caused by transitory dynamics of plastic deformation, which are highly sensitive to the material microstructure. Indeed, a tendency to periodic relaxation-type oscillations, predicted by local models of the PLC effect, disregarding strain heterogeneity, is observed for the least strain-rate value tested. In other words, the further decrease in the effective dimension of the collective dislocation dynamics occurs near the lower strain-rate boundary of instability. The entire map of behaviors is consistent with nonlocal models, combining the local property of the negative stress–strain rate sensitivity and the nonlocal spatial coupling due to internal stresses resulting from strain gradients (see, e.g., [22]). The approaches developed in these models may be useful for understanding other nonlinear systems described by N-shaped nonlinearity and containing many interacting elements, so that transitions between high-dimension modes and low-dimension modes are possible.

The analysis of the experimental data is supported by the study that shows influence of stochastic noise on multifractal Cantor sets. This investigation provides insight upon the general question of uncovering the dynamical properties in noisy experimental data. A number of other numerical techniques have been proposed previously, mostly with the aim of reconstructing deterministic chaos in low-dimensional dynamical systems [23,24]. It is shown in the present paper that the multifractal analysis can serve as a simple, practical tool apt to detect self-similarity in very noisy signals with unknown dimensionality.

It should be stressed that as the stochastic noise continuously fills the given time interval, its effect is different for

clustered and nonclustered signals. The multifractal spectra of nonclustered signals were found to be quite insensitive to noise. In contrast, the spectra of clustered signals are strongly distorted even by small noise amplitudes. A simple test based on the truncation of a time series, using a variable threshold, is proposed to verify the apparent multifractal behavior.

ACKNOWLEDGMENTS

The authors are grateful to A. Beaudoin, C. Fressengeas, A. Jacques, P. Kurath, and R. McDonald for fruitful discussions. This work was partly supported by the Russian Foundation for Basic Research through Grant No. 04-02-17140.

[1] A. Portevin and F. Le Chatelier, C. R. Hebd. Seances Acad. Sci. **176**, 507 (1923).
[2] A. A. Andronov, A. A. Vitt, and S. E. Khaikin, *Theory of Oscillators* (Pergamon, Oxford, 1966).
[3] L. P. Kubin, C. Fressengeas, and G. Ananthakrishna, in *Dislocations in Solids*, edited by F. R. N. Nabarro and M. S. Duesbery (Elsevier Science BV, Amsterdam, 2002), Vol. 11, p. 101.
[4] L. P. Kubin and Y. Estrin, Acta Metall. **33**, 397 (1985).
[5] P. Rodriguez and S. Venkadesan, Solid State Phenom. **42-43**, 257 (1995).
[6] M. A. Lebyodkin, Y. Bréchet, Y. Estrin, and L. P. Kubin, Phys. Rev. Lett. **74**, 4758 (1995).
[7] M. S. Bharathi, M. Lebyodkin, G. Ananthakrishna, C. Fressengeas, and L. P. Kubin, Phys. Rev. Lett. **87**, 165508 (2001); Acta Mater. **50**, 2813 (2002).
[8] P. Bak, C. Tang, and K. Wiesenfeld, Phys. Rev. A **38**, 364 (1988).
[9] G. Ananthakrishna, C. Fressengeas, M. Grosbras, J. Vergnol, C. Engelke, J. Plessing, H. Neuhauser, E. Bouchaud, J. Plane's, and L. P. Kubin, Scr. Metall. Mater. **32**, 1731 (1995).
[10] P. Bergé, Y. Pomeau, and C. Vidal, *Order Within Chaos, Towards a Deterministic Approach to Turbulence* (Wiley, New York, 1984).
[11] G. D'Anna and F. Nori, Phys. Rev. Lett. **85**, 4096 (2000).
[12] D. Kugiumtzis, A. Kehagias, E. C. Aifantis, and H. Neuhäuser, Phys. Rev. E **70**, 036110 (2004).
[13] A. Sarkar and P. Barat, Phys. Lett. A **367**, 291 (2007).
[14] K. Darowicki, J. Orlikowski, A. Zielin'ski, and W. Jurczak, Comput. Mater. Sci. **39**, 880 (2007).
[15] M. A. Lebyodkin and Y. Estrin, Acta Mater. **53**, 3403 (2005).
[16] M. A. Lebyodkin and T. A. Lebedkina, Phys. Rev. E **73**, 036114 (2006).
[17] T. C. Halsey, M. H. Jensen, L. P. Kadanoff, I. Procaccia, and B. I. Shraiman, Phys. Rev. A **33**, 1141 (1986).
[18] J. Feder, *Fractals* (Plenum, New York, 1988).
[19] $Z_1(\delta t)=\Sigma_i \mu_i \ln \mu_i$ for $q=1$. The same consideration as in the main text shows that Z_1 is proportional to $ln(\delta t)$ in the uniform case. Relationship (2), describing multifractal scaling laws, reads for $q=1: Z_1(\delta t) \sim D_1 \ln(\delta t)$.
[20] A. Chhabra and R. V. Jensen, Phys. Rev. Lett. **62**, 1327 (1989).
[21] J. Mach, F. Mas, and F. Sague's, J. Phys. A **28**, 5607 (1995).
[22] S. Kok, M. S. Bharathi, A. J. Beaudoin, C. Fressengeas, G. Ananthakrishna, L. P. Kubin, and M. Lebyodkin, Acta Mater. **51**, 3651 (2003).
[23] T. Schreiber, Phys. Rev. E **47**, 2401 (1993).
[24] M. Strumik, W. M. Macek, and S. Redaelli, Phys. Rev. E **72**, 036219 (2005).